CHAPTER TWO

Synthesis and application of Ormosil film in presence of TiO_2 and Pd linked glycidoxypropyltrimethoxy silane

This chapter deals with synthesis and characterization of Ormosil-TiO_2-Pd film in presence of potassium ferricyanide and ferrocene methanol and investigations have been made to verify the quality of present nanocomposite material in the development of amperometric sensor for ascorbic acid.

2.1. INTRODUCTION

The chemistry associated to the sol-gel process is compatible with the reaction involved in organic chemistry, making possible the preparation of organic-inorganic hybrid having the potentials for providing unique combination of properties [Jung et al., (2012)]. The greatest interest in these materials however, arises because most of them can be manufactured quite easily at room temperature by sol-gel processing via the hydrolysis and condensation of alkoxysilane precursors having organic functionality. Such precursors after following sol-gel process leads to the formation of organically modified silicate (ormosil). Organic functionality during sol-gel process could be used to increase the degree of cross linking and improve film adhesion to its surface. The simple preparation protocol of solids displaying a very large diversity of chemical composition, structure and tailor made properties and the possibility to synthesize thin film; the ability to immobilize specific material within the silica matrix while maintaining their activity make organically modified silicates (ormosils) preferable for encapsulation of materials. Modification in sol-gel precursor provides better way of controlling nanoporous geometry of sol-gel glasses suitable for sensor design.

This concept has led to the prediction of wide variety of composite of organically modified silicate of special interest from two reasons. First, they allow the encapsulation of catalysts with effective retention properties in case of strong interaction with the organic branch, or better the covalent bonding of a charge transfer cofactor to the composite material via chemical reaction with previously grafted groups. Second, it is possible to tone the wettability of composite material by a judicious choice of the ratio between hydrophilic and hydrophobic monomers allowing precise control of the nanostructured domains enabling the encapsulation of electron transfer mediators like ferrocene monocarboxylic acid that has shown potential application in realizing the electron exchange during bioelectrochemical sensing [Pandey et al. (2007)]. Two combinations of these hydrophobic and hydrophilic alkoxysilanes e.g. (1)

3-glycidoxypropyltrimethoxysilane (3-GPTMS) and trimethoxysilane (TMS); (2) 3-Aminopropyltrimethoxysialne (3-APTMS) and 2-(3,4-epoxycyclohexyl) ethyltrimethoxysilane (ECETMS); in appropriate ratio were used for encapsulating the ferrocene monocarboxylic acid (Fc-COOH) [Pandey et al., (2005a); Pandey and Upadhyay, (2005a)]. The redox electrochemistry of ormosil-encapsulated Fc-COOH in both cases was found to display sluggish reversible electrochemistry mainly due to restricted mobility of ferrocenium ions within nanostructured domain. In addition to that Fc-COOH loses its mediation capability within nanostructured domains required for designing mediated electrochemical sensors [Pandey et al., (2001d) Pandey et al. (2001)]. These findings directed our attention to overcome these limitations and to design the nanostructure system fulfilling the requirement of ferrocene-mediated bioelectrochemical sensing and the choice of electrocatalyst in combination with encapsulated mediator for facilitating electron transfer process became significant. Fortunately novel finding on the interaction of palladium chloride and GPTMS was observed while making ormosil film with TMS [Pandey et al., (1999c); Pandey et al., (2001d)]. The presence of palladium chloride / tetrachloro palladate ($PdCl_2$ /K_2PdCl_4) opens the epoxide ring of glycidoxy-residue and in turn gets reduced into palladium followed by subsequent co-ordination within two glycidoxy residue [Pandey et al., (2001d)]. When such palladium linked-GPTMS and TMS were used for encapsulating ferrocene derivative within ormosil film, the redox electrochemistry of the ferrocene monocarboxylic acid showed excellent reversible electrochemistry even better than that of the same recorded in homogeneous solution. In addition to that the resulting nanostructured thin film was efficient for catalyzing the re-generation of redox enzyme during mediated bioelectrochemical sensing [Pandey et al., (1999b); Pandey et al., (1999d)]. Such improvement in redox electrochemical behavior of mediator was found to be function of two main events; (1) formation of Pd-glymo complex and, (2) formation of Pd-Si linkage between trimethoxysilane and palladium chloride resulting the formation of silicate matrix as solid-solution [Pandey et al.,

(2001d)]. Accordingly the choice of GPTMS and TMS yielded novel biomaterial of silicate useful in potential electrocatalysis [Pandey et al., (2001a); Pandey and Upadhyay, (2005b); Pandey et al., (1999b)]. However, the choice of 3-APTMS and ECETMS in ormosil film preparation provided excellent opportunity for controlling the hydrophobic and hydrophilic components with additional possibility of manipulating the silicate matrix with other metal nanoparticles and known materials [Pandey and Upadhyay, (2005a)] for electroanalytical applications. These findings enabled for generating a library of electrocatalytic sited within such nanostructured domains for specific applications [Pandey and Singh, (2008)]. One of the problems in precise control of electrocatalytic activity within such matrix was linked to the thickness of the ormosil matrix. An increase in the thickness of the ormosil film caused decrease in electrocatalytic behaviour and directed our attention to overcome such limitation. The finding on the role of titanium (Ti) has shown the possibility for overcoming such limitation [Bao-Ling and Li-Li, (2004); Sorek et al., (1995)]. Accordingly, we intended to investigate the development of ormosil film from the suspension of alkoxysilane precursors along with the suitable suspension of titania. In addition to that such combinations also allowed the encapsulation of suitable fraction of palladium-glymo complex along with other metal oxide sol during sol–gel processing. These observations expanded our attention to examine the role of encapsulated titania in the presence and absence of palladium for studying the redox electrochemistry of ferrrocene methanol and potassium ferricyanide encapsulated within nanostructured matrix of ormosil. The redox electrochemistry of these functionalised ormosil electrodes and their application in the electrocatalytic oxidation of ascorbic acid based on cyclic voltammetry, amperometry and chronoamperometric measurements are reported in this chapter.

L (+)-ascorbic acid (AA) (widely known as Vitamin C) is one of the most important food constituents distributed widely in both plant and animal kingdoms. It takes part in some important biological reactions such as free

radical scavenging, cancer prevention and improving immunity. A recommended daily dose of AA is about 70–90 mg. Inadequate intake would result in the symptoms of scurvy, gingival bleeding etc; excess AA intake may lead to urinary stone, diarrhea and stomach convulsion [Zuo, Xia et al., (2012)]. Therefore, it is of great importance to have suitable methods for the determination of AA. Several traditional methods are used, such as spectrophotometry [Absalan et al., (2012)], fluorimetry [Psaila et al., (2012)], chromatography [Huang, Tina H. et al., (2007); Szultka et al., (2014); Wabaidur et al., (2013)] and redox titration [Huang, Tina H. et al., (2007)]. These methods require complex sample pretreatment and expensive apparatus. Thus, the development of easy and inexpensive method for the rapid determination of AA is very important for pharmaceutical and food chemistry, as well as for the physiological and medical research. Electrochemical methods are more powerful tool for the determination of AA as it is an electroactive molecule [Shi et al., (2012)]. The direct oxidation of AA over bare electrodes suffers several problems like electrode fouling, poor reproducibility, high value of overpotential and interference of other oxidizable biomolecules (catecholamine, uric acid etc). In order to resolve these problems, the electrode surface was modified with various materials for the electrocatalytic oxidation of AA. Modified electrodes provide a promising method to overcome all the limitations of bare electrodes. For present investigation we have chosen TiO_2 along with palladium linked-GPTMS in the presence of potassium ferricyanide and ferrocene methanol along with ormosil matrix modified on glassy carbon electrode surface to make a comparative study on the electrocatalysis of AA.

2.2. EXPERMENTAL

2.2.1. Materials

Titanium isopropoxide, $PdCl_2$, 3-Aminopropyltrimethoxysilane (3-APTMS), 2-(3,4-epoxycyclohexyl)ethyltrimethoxysilane (epoxy silane), 3-

glycidoxypropyltrimethoxysilane (3-GPTMS), were obtained from Sigma-Adrich Chem. India; Isopropanol and HCl were obtained from E-Merck. All the experiments were performed at room temperature.

2.2.2. Synthesis of TiO_2 and Pd Sol

$Ti(OH)_4$ sol and palladium linked glycidoxypropyltrimethoxysilane (Pd-glymo) sol were used as a source of TiO_2 and Palladium during sol-gel processing of ormosil-coated electrode. $Ti(OH)_4$ sol was prepared as follow: 7 ml of 0.5 M titanium isopropoxide was added dropwise into HCl (0.1 M). The resulting solution was peptized overnight followed by dialysis for 3 days in order to eliminate any residual acid and Cl ion that leads to the formation of transparent $Ti(OH)_4$ sol [Sugimoto and Zhou, (2002); Wang, Guang-Li et al., (2009)]. Whereas Pd-glymo complex suspension was made by adding 25µL aqueous solution of (1mg/mL) palladium chloride with 50 µl of 3-glycidoxypropyltrimethoxysilane [Pandey et al., (2001a)].

2.2.3. Instrumentation

Surface morphology and nanogeometry of ormosil films was determined by Veeco Nanoscope IV multimode AFM (Veeco Metrology group, Santa Barbara, CA). Chemical composition of ormosil films was measured by Energy dispersive spectroscopic (EDS) analysis was conducted with ZEISS SUPRA 40 Scanning Electron Microscope (SEM) coupled to an Energy Dispersive spectrometer. Thicknesses of films were measured by ellipsometer from Gaertner scientific corporation. The UV–visible spectra were recorded using a Systronics UV–VIS Double Beam Spectrophotometer 2201. The absorbance spectrum was monitored between 200–800 nm.

Electrochemical experiments were performed on an Electrochemical Workstation Model CHI660B, CH Instruments Inc., TX, USA, in a three-electrode configuration with a working volume of 3 mL. An Ag/AgCl electrode (Orion, Beverly, MA, USA) and a platinum plate electrode served as reference and counter electrode, respectively. All potentials given below are relative to the Ag/AgCl. The working electrode was a glassy carbon disc (2 mm diameter) and a silicon wafer (1 cm^2). The later was utilized for characterization

purposes. The electrodes were ultrasonically cleaned in water for 5 min to remove any adherent impurity.

2.2.4. Fabrication of organically modified electrodes

The organically modified silicate film was made on a polished glassy carbon electrode obtained from bioanalytical system (West Lafayette, IN; (MF 2010)). The thin film of ormosil on gassy electrode surface was casted from the homogeneous suspension of a mixture of functional alkoxysilanes namely 3-aminopropyltrimethoxysilane (3-APTMS) and 2-(3,4-epoxycyclohexyl) ethyltrimethoxysilane along with TiO_2 and Pd sol as describe in Table 1. The suspensions of these sols are homogenized by ultrasonication and an amount of 5µL of each one was dropped separately on clean GCE followed by drying at 25–30 °C for 2-3 h. The presence of either ferrocene methanol or potassium ferricyanide in homogenous suspension resulted into fabricating six types of ormosil coated electrodes in three different system as; (i) ormosil; (ii) Ormosil-TiO_2; (iii) Ormosil-TiO_2-Pd. These are referred as follows in table 2.1.

Table 2.1. The composition of six different types of ormosil electrodes.

System	A (µL)	B (µL)	C (µL)	D (µL)	E (µL)	F (µL)	G (µL)
Ormosil(Ferri)	20	5	25	100	-	5	-
Ormosil-TiO_2(Ferri)	20	5	25	50	50	5	-
Ormosil-TiO_2-Pd(Ferri)	20	5	25	-	50	5	50
Ormosil(FM)	20	5	25	100	-	5	-
Ormosil-TiO_2(FM)	20	5	25	50	50	5	-
Ormosil-TiO_2-Pd(FM)	20	5	25	-	50	5	50

A- 3-APTMS; **B-** 2-(3,4-epoxycyclohexyl)ethyltrimethoxysilane; **C-** aqueous solution of 1 mM $K_3Fe(CN)_6$ (Ferri) or Ferrocene methanol (FM); **D-** Double

distilled water; **E-** 0.5M $Ti(OH)_4$ sol; **F-** HCl (0.1 M**)**; **G-**diluted 3-GPTMS linked $PdCl_2$**.**

2.3. RESULTS AND DISCUSSION

2.3.1. AFM and SEM Analysis

The first stage of the investigation is to understand the morphological as well as the structural behaviour of as prepared Ormosil films. Figure 2.1 A, B and C shows the typical AFM images of Ormosil, Ormosil-TiO_2 and Ormosil-TiO_2-Pd respectively. The AFM images clearly depict a better and ordered nanogeometry of Ormosil-TiO_2-Pd film as compared to that of Ormosil and Ormosil-TiO_2 films. The Figure 2.1 (B and C) shows the AFM images of Ormosil-TiO_2 and Ormosil-TiO_2-Pd, Significant change in morphology is recorded with ordered nanostructured domain in case of representing the encapsulation of TiO_2 and TiO_2-Pd present in nanostructure domain of Ormosil-TiO_2-Pd film. The morphology of Ormosil-TiO_2-Pd film further validate by SEM analysis. The SEM image of Ormosil-TiO_2-Pd film shown in Figure 2.2 also justifying ordered nanostructured geometry of Ormosil-TiO_2-Pd film.

2.3.2. EDS Analysis

Energy dispersive spectroscopy (EDS) has been attempted for the elemental analysis of as prepared ormosil films. Figure 2.3 shows the photograph of ormosil films on silicon wafer and EDS spectra of Ormosil, Ormosil-TiO_2, Ormosil-TiO_2-Pd respectively. The EDS spectra indicate the presence of the characteristic peaks assigned to the carbon, nitrogen and oxygen. It has been also found that the characteristic Si peak is present in all spectrums, mirroring the presence of silica matrix. Beside this, the existence of titanium and titanium with palladium (EDS spectra of Ormosil-TiO_2, Ormosil-TiO_2-Pd respectively) validate the incorporation of same in ormosil matrix. Furthermore, the percentage atomic contents of these films were also presented (bottom portion of respective figures) for precise comparison.

2.3.3. Ellipsometry

Figure 2.4 shows the photo of ellipsometer and ormosil films casted over glass surface for the analysis. Thicknesses of films were measured and found to be in order of 2200 nm, 1590 nm and 800 nm for Ormosil, Ormosil-TiO_2, and Ormosil-TiO_2-Pd respectively. The incorporation of TiO_2-Pd resulted into excellent thin film to the order of 800 nm and reflects the success of our programme on the role of TiO_2 and TiO_2-Pd during thin film casting.

2.3.4. UV-Visible Analysis

A UV-visible spectrum and photographs of Ormosil, Ormosil-TiO_2, and Ormosil-TiO_2-Pd films on glass substrate are shown in Figure 2.5. Ormosil film shows an absorbance below 300 nm. Ormosil-TiO_2 film have absorption below 370 nm is due to the excitation of electrons from the valence band to the conduction band of TiO_2 in Figure 2.5 (2). Pure anatase crystalline powder has an intense absorption band at 335 nm. Absorbance of TiO_2 represents total transparency between 368–800 nm whereas the Ormosil-TiO_2-Pd film spectra in Figure 2.5(3) shows absorbance within same range of wavelength due the presence of Pd.

2.3.5. Electrochemical analysis

The next stage of investigation concerns to justify the role of TiO_2 and Pd in electroanalytical applications. At first instant it is necessary to understand their role on the redox electrochemistry of electron transfer relays when encapsulated within ormosil film. We have already investigated in details on the interaction of palladium chloride and 3-GPTMS and the research findings confirmed the reduction of palladium (II) into Palladium [Pandey et al., (2003a); Pandey et al., (2001a)]. These materials have been used for designing ormosils films encapsulating redox species justifying improved redox electrochemistry of surface confined mediator [Pandey et al., (2003b); Pandey et al., (2001a)]. Such findings directed our attention to understand the redox behavior of mediators in the presence of metal oxide. Interestingly, we found that the encapsulation of metal oxide and its nanocomposite particularly TiO_2

and TiO_2-Pd provide significant improvement in redox electrochemistry of mediators. Figure 2.6 shows the voltammogram of Ormosil(Ferri) (a), Ormosil-TiO_2(Ferri) (b) and Ormosil-TiO_2-Pd(Ferri) (c) electrode in phospahate buffer (0.1M, pH 7.0) containing 0.5 M KCl at various scan rates between 0.01 and 0.5 V s^{-1}. The peak separation has been found to be 203 mV for ormosil, 191 mV for ormosil-TiO_2 and 103 mV for ormosil-TiO_2-Pd under similar conditions justifying improvement in reversible redox behaviour of encapsulated potassium ferricyanide within nanostructured domains as a function of TiO_2 and TiO_2-Pd content. In order to further validate the electrochemical observation, similar investigation on Ferrocene methanol has also been undertaken. The results as shown in Figure 2.8 clearly demonstrate gradual improvement in redox electrochemistry of ferrocene methanol as; ormosil-TiO_2-Pd (c) > ormosil-TiO_2 (b) > ormosil (a) similarly as illustrated for potassium ferricyanide. The peak separation values are found to be 59, 78 and 109 mV for ormosil-TiO_2-Pd(FM), ormosil-TiO_2(FM) and ormosil films(FM).

The electrochemical investigation based on cyclic voltammetry demonstrated better electrochemical behaviour of ormosil-TiO_2-Pd film. The cathodic and anodic peak current density of both mediators is plotted as a function of scan rate as well as square root of scan rate. The results presented in Figure 2.7 (a) and (b) show the charge transfer characteristic of potassium ferricyanide within nanostructured matrix. The peak current density are found to be linear upto the scan rate of 100 mV s^{-1} thereafter become nonlinear, revealing the surface confined redox process. Likewise, the result as shown in Figure 2.9 a and b justify that the peak current density increased linearly with increase in scan rate up to 150 mV s^{-1} indicating charge transport from a surface-confined redox species. These finding predict better redox behaviour of ferrocene methanol as compared to that of potassium ferricyanide.

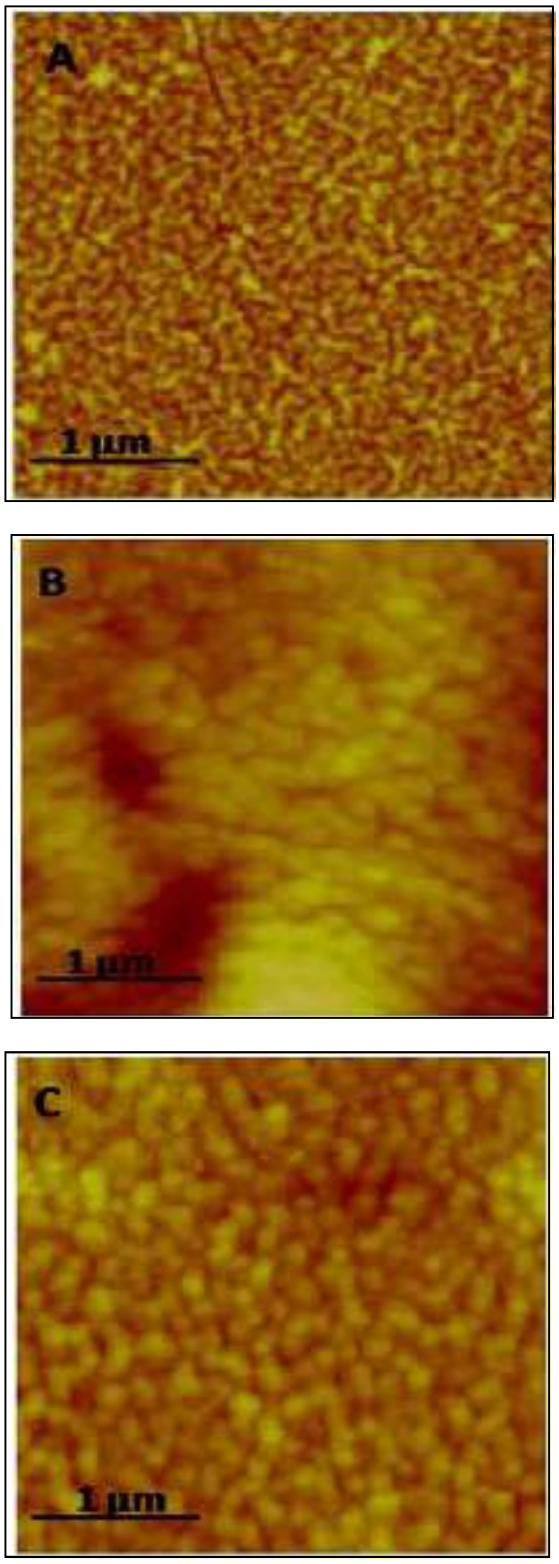

Figure 2.1. AFM image of ormosil **(A),** ormosil-TiO_2 **(B)** and ormosil-TiO_2- Pd **(C)** films.

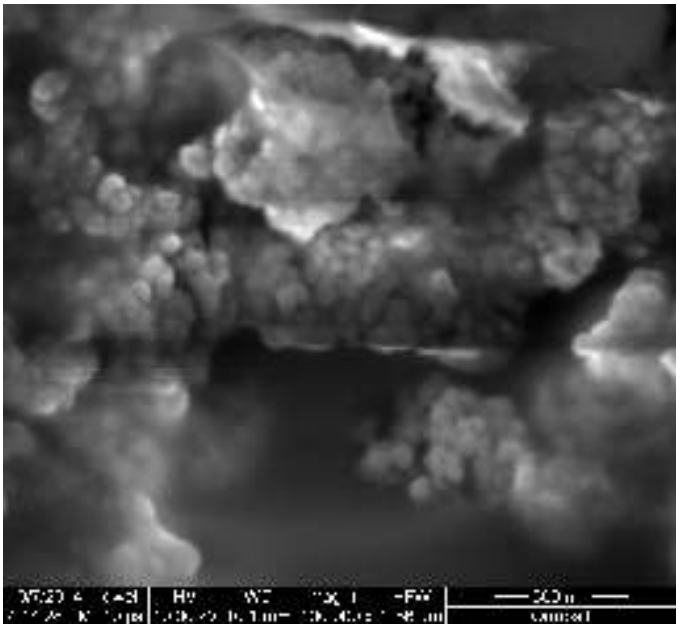

Figure 2.2. SEM image of ormosil-TiO_2- Pd film.

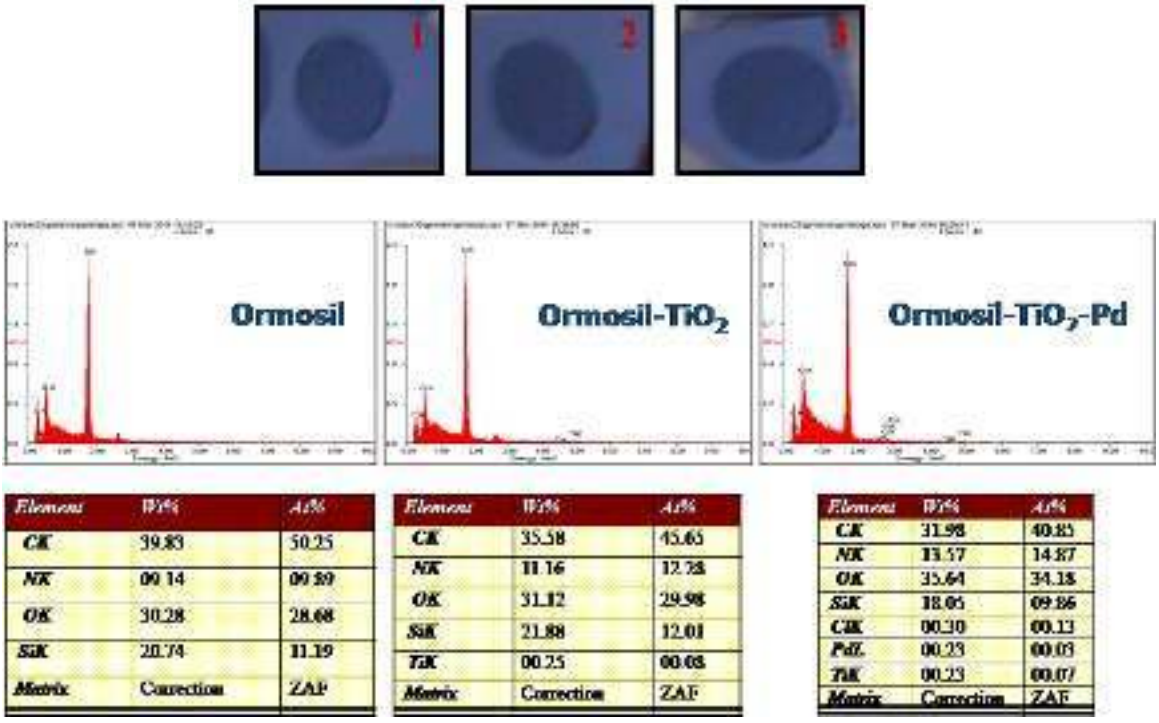

Element	Wt%	At%
CK	39.83	50.25
NK	09.14	09.89
OK	30.28	28.68
SiK	20.74	11.19
Matrix	Correction	ZAF

Element	Wt%	At%
CK	35.58	45.65
NK	11.16	12.28
OK	31.12	29.98
SiK	21.88	12.01
TiK	00.25	00.08
Matrix	Correction	ZAF

Element	Wt%	At%
CK	31.98	40.85
NK	11.57	14.87
OK	35.64	34.18
SiK	18.05	09.86
ClK	00.30	00.13
PdL	00.23	00.03
TiK	00.23	00.07
Matrix	Correction	ZAF

Figure 2.3. Energy dispersive spectroscopy of ormosil**,** ormosil-TiO_2 and ormosil-TiO_2- Pd films. The corresponding elemental analysis is shown on bottom and photographs of ormosil films on top of respective EDS images.

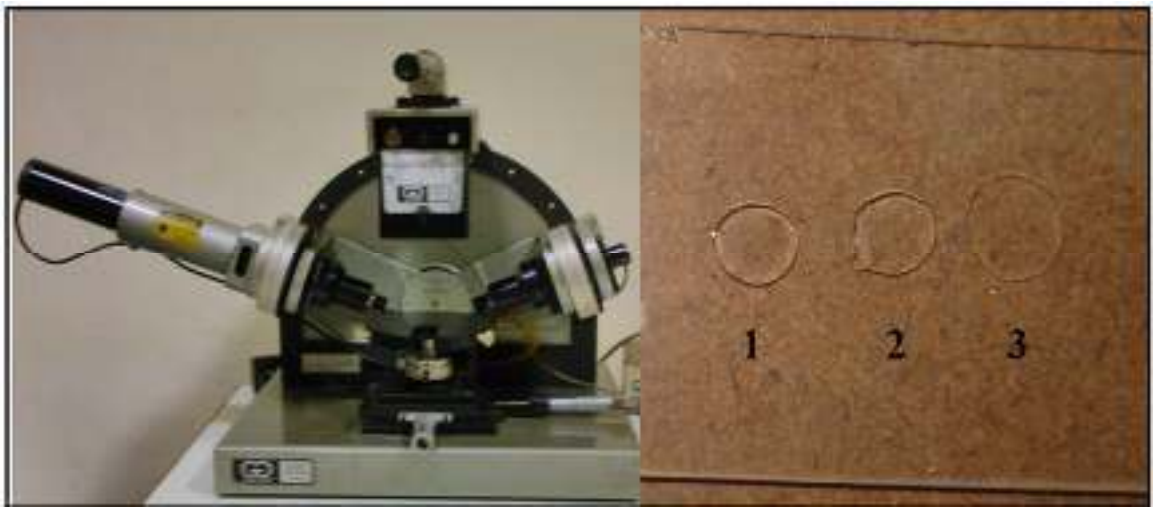

Figure 2.4. Ellipsometer and photographs of ormosil films on glass substrate.

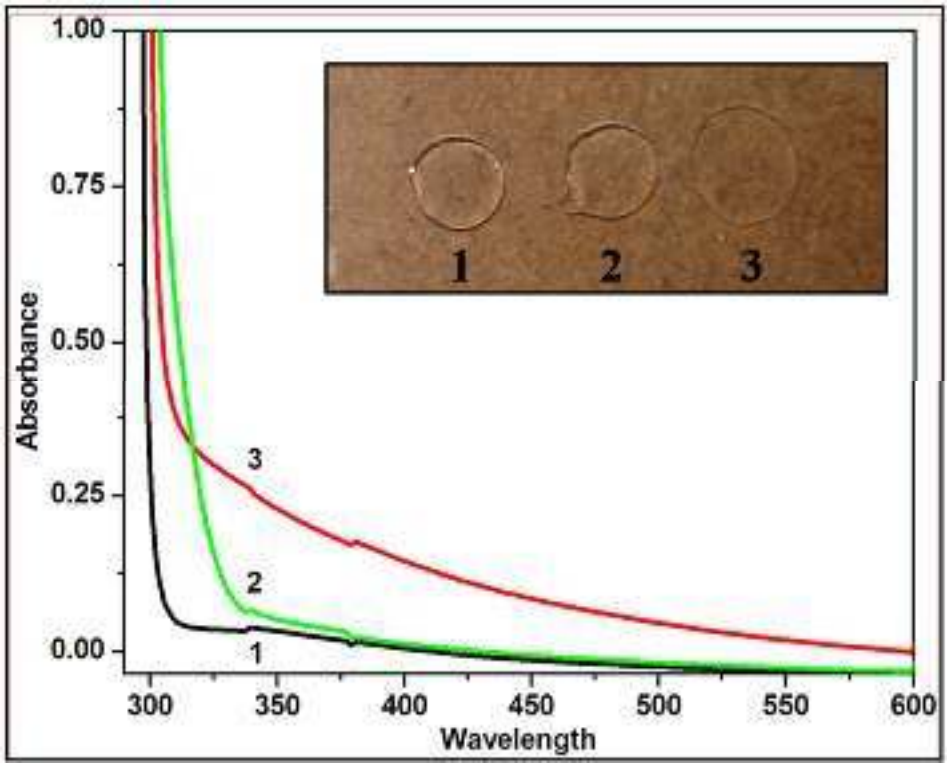

Figure 2.5. UV-Visible absorption spectrum of ormosil (1), ormosil-TiO2 (2) and ormosil-TiO2- Pd (2) films and inset shows their corresponding photographs.

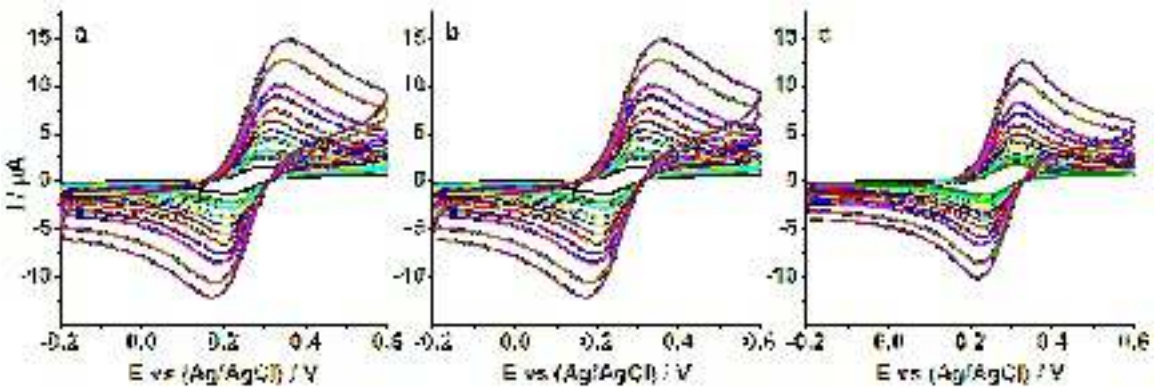

Figure 2.6. Cyclic voltammogram of **(a)** Ormosil(Ferri), **(b)** Ormosil-TiO_2(Ferri) and **(c)** Ormosil-TiO_2-Pd(Ferri) electrode in phospahate buffer (0.1M, pH 7.0) containing 0.5 M KCl at various scan rates between 0.01 and 0.5 V s^{-1}.

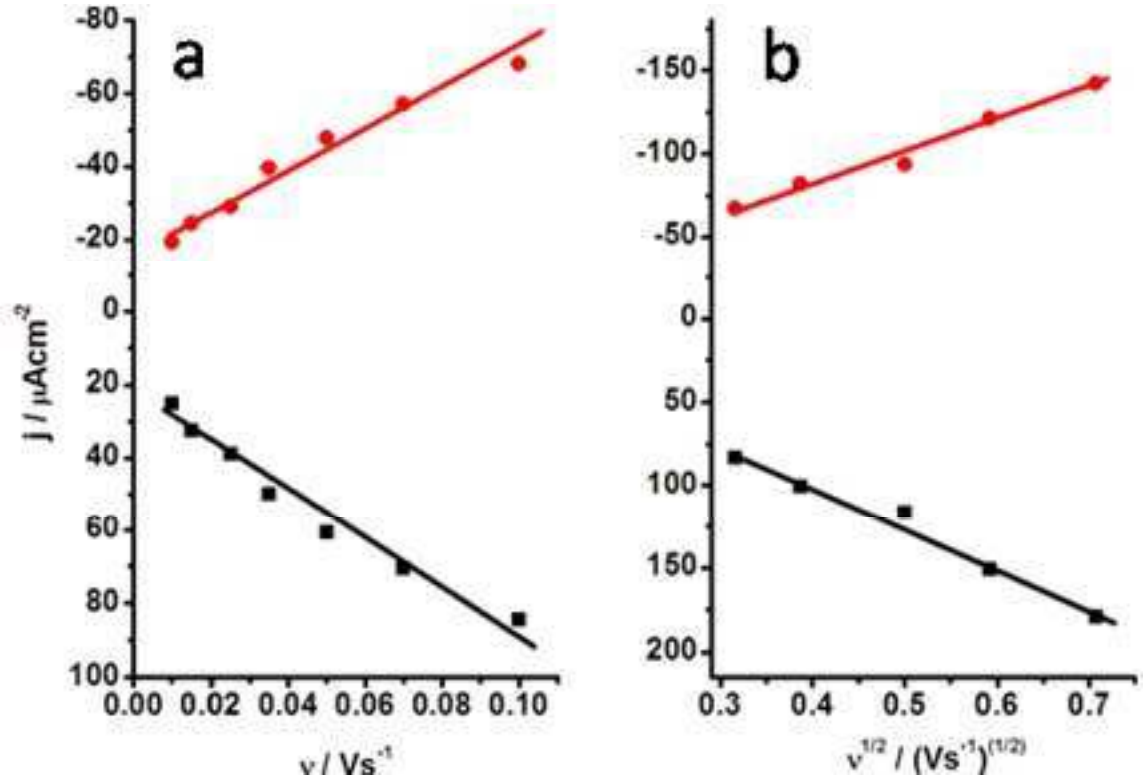

Figure 2.7. A plot of anodic and cathodic peak current density vs scan rate **(a)** and the plot of anodic and cathodic peak current density vs square root of scan rate **(b)** for Ormosil-TiO_2-Pd(Ferri).

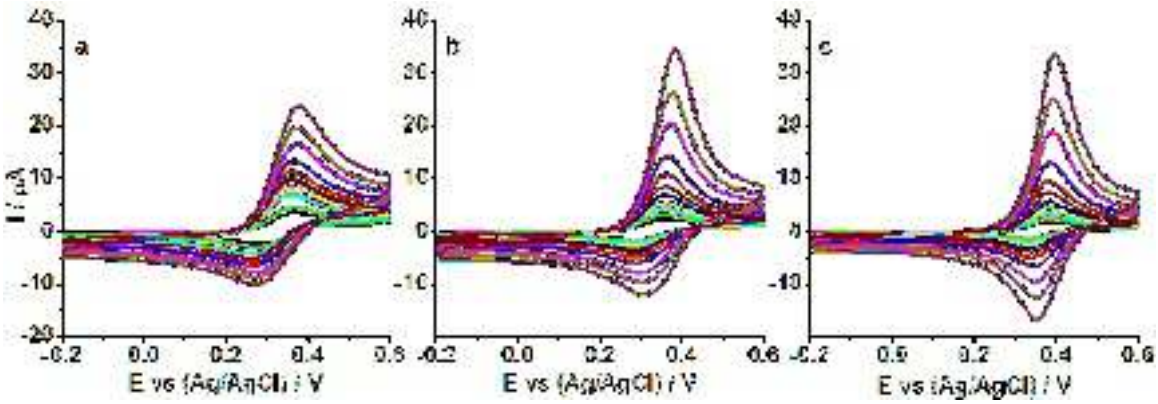

Figure 2.8. Cyclic voltammogram of **(a)** Ormosil(FM), **(b)** Ormosil-TiO_2(FM) and **(c)** Ormosil-TiO_2-Pd(FM) electrode in phospahate buffer (0.1M, pH 7.0) containing 0.5 M KCl at various scan rates between 0.01 and 0.5 V s^{-1}.

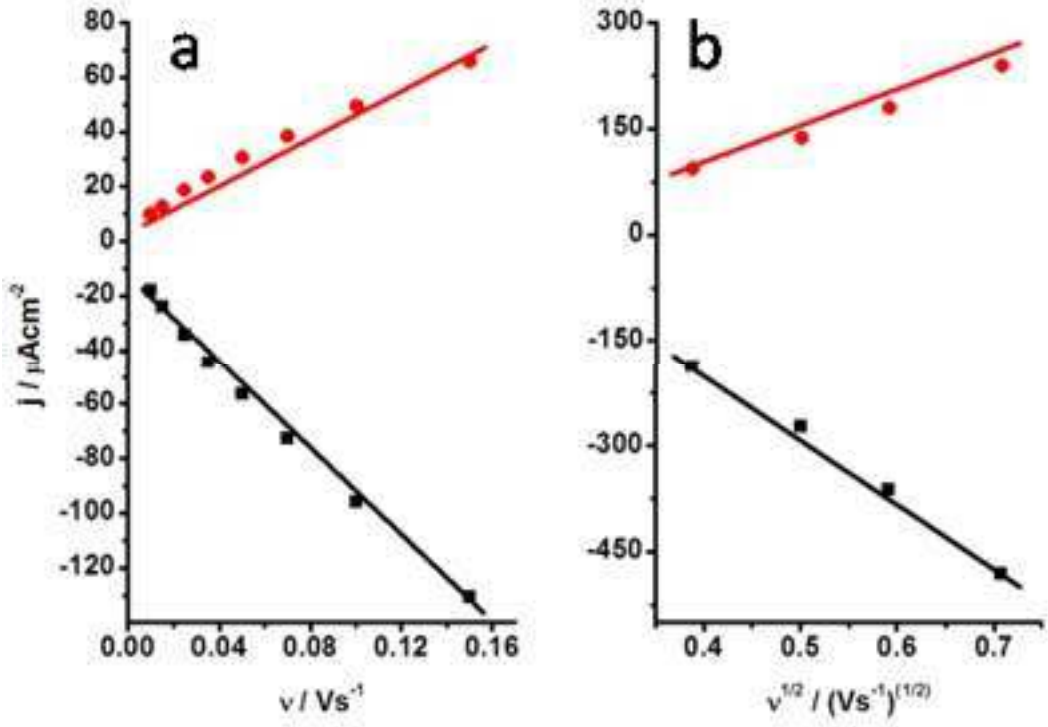

Figure 2.9. A plot of anodic and cathodic peak current density vs scan rate **(a)** and the plot of anodic and cathodic peak current density vs square root of scan rate **(b)** for Ormosil-TiO_2-Pd(FM).

2.3.6. Role of encapsulated electron transfer mediators with in nanostructured domains of organically modified silicate

The aim of the present investigation is to understand the electrochemistry of ferrocene methanol and potassium ferricyanide when encapsulated within the nanostructured domains of ormosil film and to justify the electrocatalytic property of the same. At first instant it is important to understand the significance of ormosil encapsulated mediator from those of the same recorded with that of soluble mediator. Accordingly we investigated the electrochemistry of soluble ferrocene methanol in aqueous solution in absence and the presence of ascorbic acid and compared to that of recorded with encapsulated ferrocene methanol within ormosil film under similar conditions. Figure 2.10 A shows the cyclic voltammetry of ferrocene methanol in aqueous solution in absence (1) and the presence (2) of 1 mM ascorbic acid. The electrochemical behaviour of ferrocene methanol is similar to that recorded by Bard et al. [34]. Figure 2.10 B shows the results recorded on ferrocene methanol when encapsulated within ormosil film. The results on the electrochemical sensing of ascorbic acid justify variable role of ferrocene methanol when present in solution and ormosil matrix. A plot of current function (peak current/square root of scan rate) vs. square root of scan rate has been constructed for evaluating the performances of ferrocene methanol present under two different conditions (Figure 2.10 A and B). The insets to Figure 2.10 A and B show the diagnostic plots and provide valuable information on electrochemical sensing of ascorbic acid. When ferrocene methanol is present in homogeneous phase (Figure 2.10 A), there is decrease in current function with an increase in scan rate justifying the mediated mechanism during electrochemical sensing (inset to Figure 2.10 A). On the other hand when the mediator is encapsulated within ormosil film redox electrocatalysis instead of mediated mechanism is recorded (inset to Figure 2.10 B). Such finding revealed the role of ormosil encapsulated mediator and support its potentiality of modified film for electrochemical sensor design.

2.3.7. *Evaluation of electrocatalytic ability of ormosil modified films towards AA oxidation*

2.3.7.1. *Cyclic voltammetry*

A need of neutral pH is necessary for the oxidation of AA performed in an electrolyte solution. The cyclic voltammograms for the oxidation of ascorbic acid on Ormosil(Ferri), Ormosil-TiO_2(Ferri) and Ormosil-TiO_2-Pd(Ferri) are shown in Figure 2.11 (a-c) respectively. There is an increase in anodic current close to 0.3V on the addition of AA as a function of TiO_2, and TiO_2-Pd in the order of Ormosil-TiO_2-Pd(Ferri) > Ormosil-TiO_2(Ferri) > Ormosil(Ferri) explaining the contribution of TiO_2 and TiO_2-Pd on electrocatalytic oxidation of AA.

Furthermore, the role of TiO_2 and TiO_2-Pd was also studied with ferrocene methanol as mediator in ormosil film under similar conditions. Figure 2.12 (a-c) shows the voltammograms of Ormosil(FM), Ormosil-TiO_2(FM) and Ormosil-TiO_2-Pd(FM) respectively in absence (1) and the presence (2) of 1mM AA. The results are similar as that recorded for potassium ferricyanide with significant increase in anodic current revealing more efficient catalytic behaviour of ferrocene methanol as compared to that of potassium ferricyanide. Remarkable improvement in anodic current on the addition of same concentrations of AA justifies the advantages of Ormosil-TiO_2-Pd(FM) in AA analysis. The results again validate that ormosil alone is least sensitive to AA (Figure 2.11 a and Figure 2.12 a) with gradual increase in electrocatalytic property as function of TiO_2 (Figure 2.11 b and Figure 2.12 b) and TiO_2-Pd (Figure 2.11 c and Figure 2.12 c).

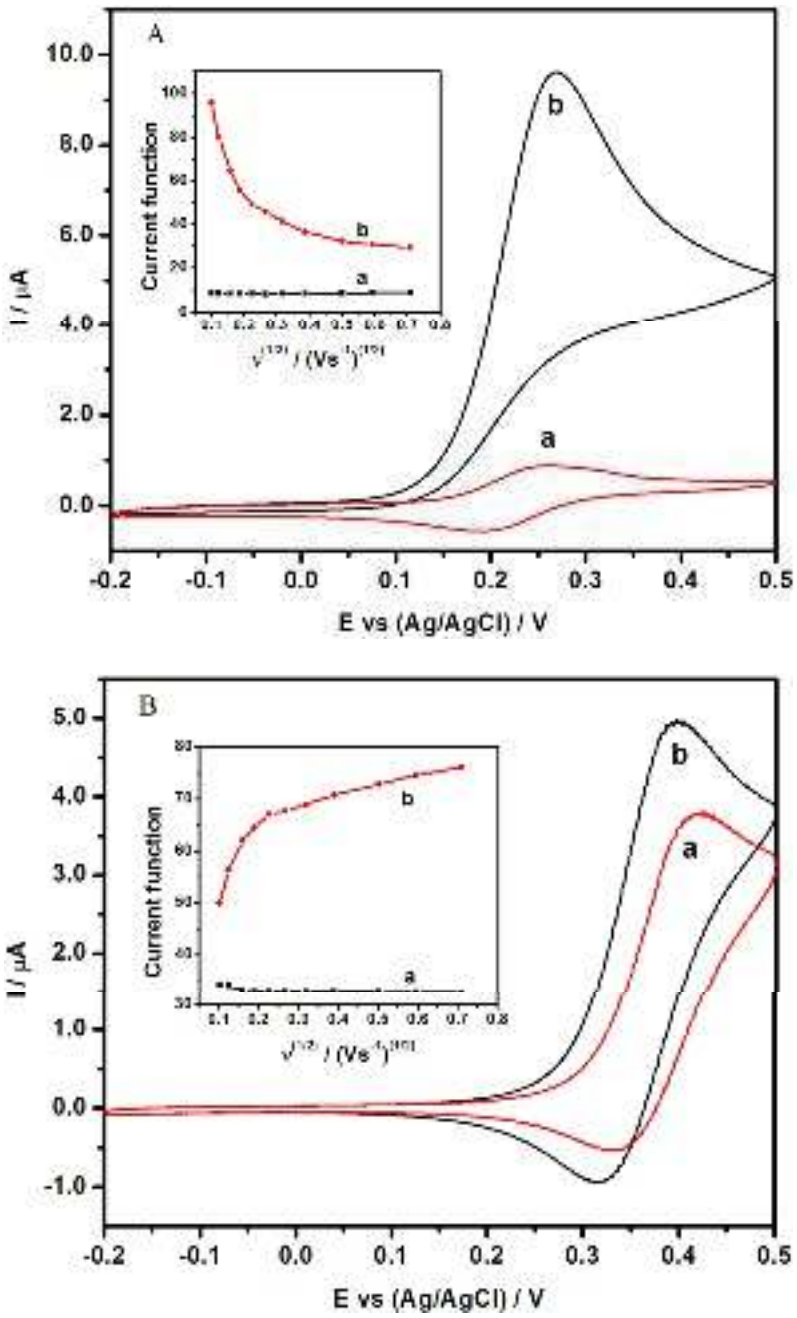

Figure 2.10. (A) Cyclic voltammogram of aqueous solution of ferrocene methanol (1mM) in phosphate buffer (0.1 M, pH 7.0) containing 0.5 M KCl at the scan rate of 0.01 Vs^{-1} in absence **(a)** and the presence of 1 mM ascorbic acid **(b)**; **(B)** cyclic voltammogram of ferrocene methanol encapsulated within ormosil film in phosphate buffer (0.1 M, pH 7.0) containing 0.5 M KCl at the scan rate of 0.01 V s^{-1} in absence **(a)** and the presence of 1 mM ascorbic acid **(b)**; insets to figure show the plot of current function vs. square root of scan rates for soluble ferrocene methanol (inset to **(A)**) and ormosil encapsulated ferrocene methanol (inset to **(B)**).

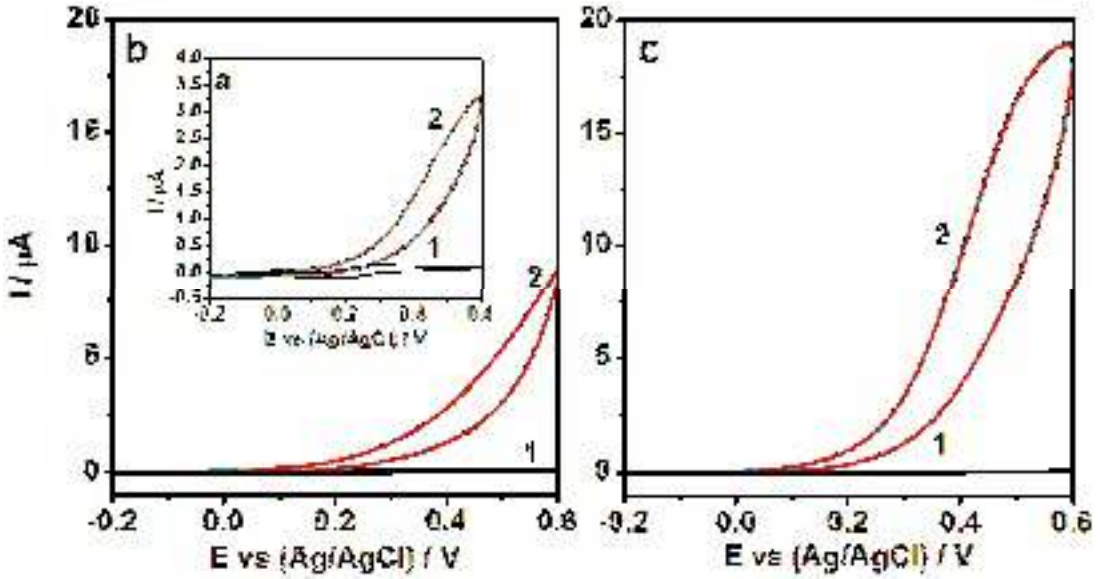

Figure 2.11. Cyclic voltammogram of **(a)** Ormosil(Ferri), **(b)** Ormosil-TiO_2(Ferri) and **(c)** Ormosil-TiO_2-Pd(Ferri) electrode in absence **(1)** and presence **(2)** of 1 mM AA in phosphate buffer (0.1M, pH 7.0) containing 0.5 M KCl at the scan rate of 10 mV/s.

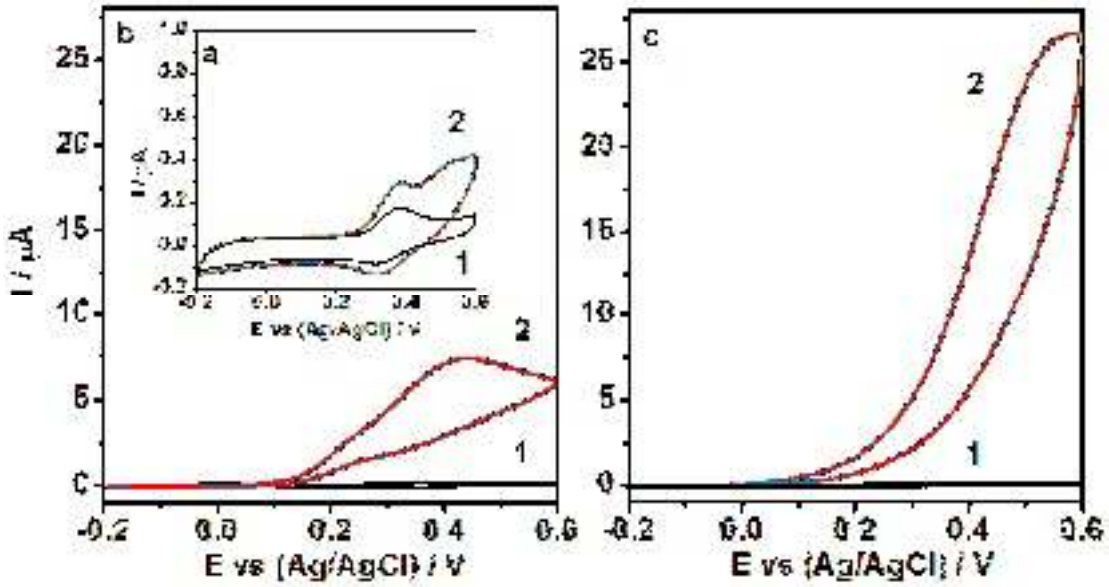

Figure 2.12. Cyclic voltammogram of **(a)** Ormosil(FM), **(b)** Ormosil-TiO_2(FM) and **(c)** Ormosil-TiO_2-Pd(FM) electrode in absence **(1)** and presence **(2)** of 1 mM AA in phospahate buffer (0.1M, pH 7.0) containing 0.5 M KCl at the scan rate of 10 mV/s.

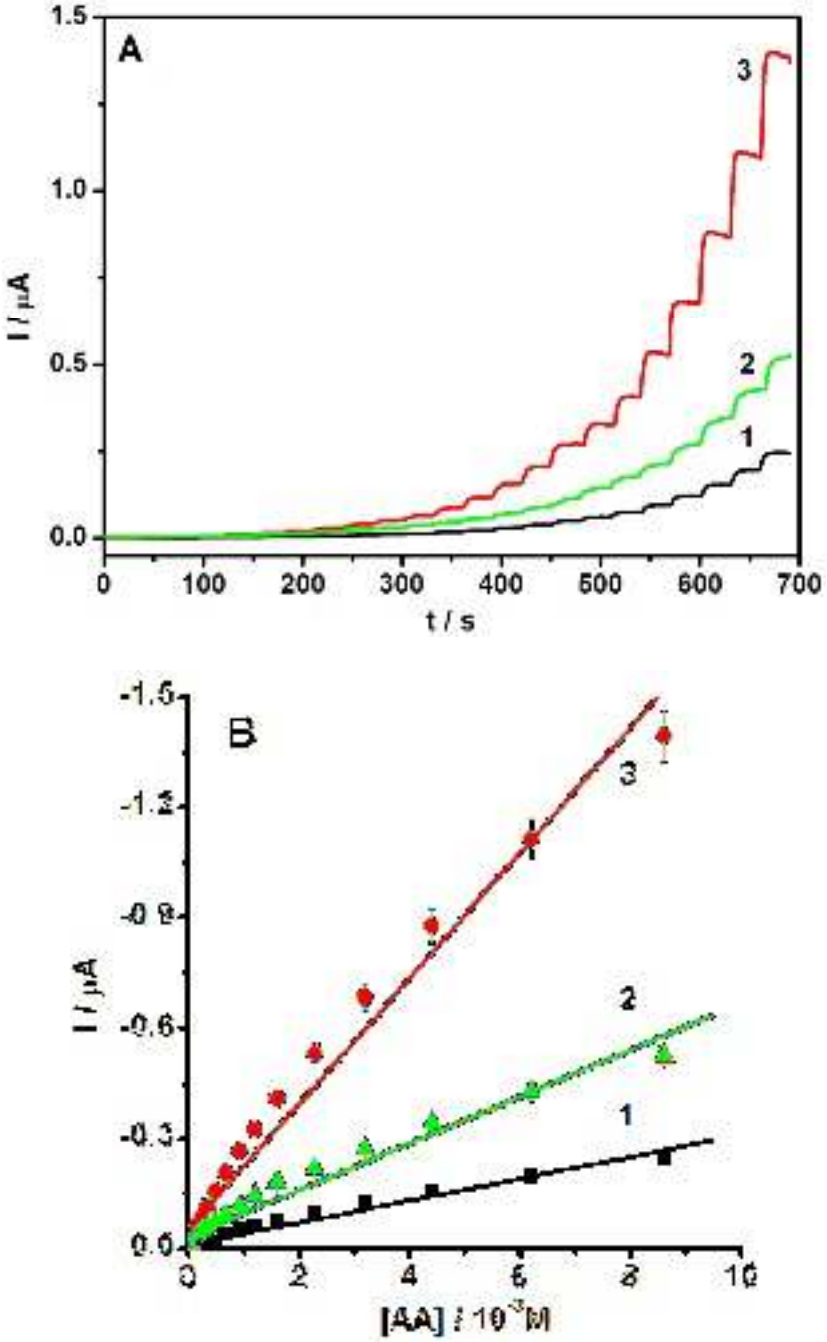

Figure 2.13. (A) Amperometric responses of **(1)** Ormosil(Ferri), **(2)** Ormosil-TiO_2(Ferri) and **(3)** Ormosil-TiO_2-Pd(Ferri) systems on the addition of varying concentrations (10 nM to 5 mM) of AA in 0.1 M phosphate buffer(pH 7.0) at 0.3V vs. Ag/AgCl; **(B)** show the corresponding calibration curves for AA analysis.

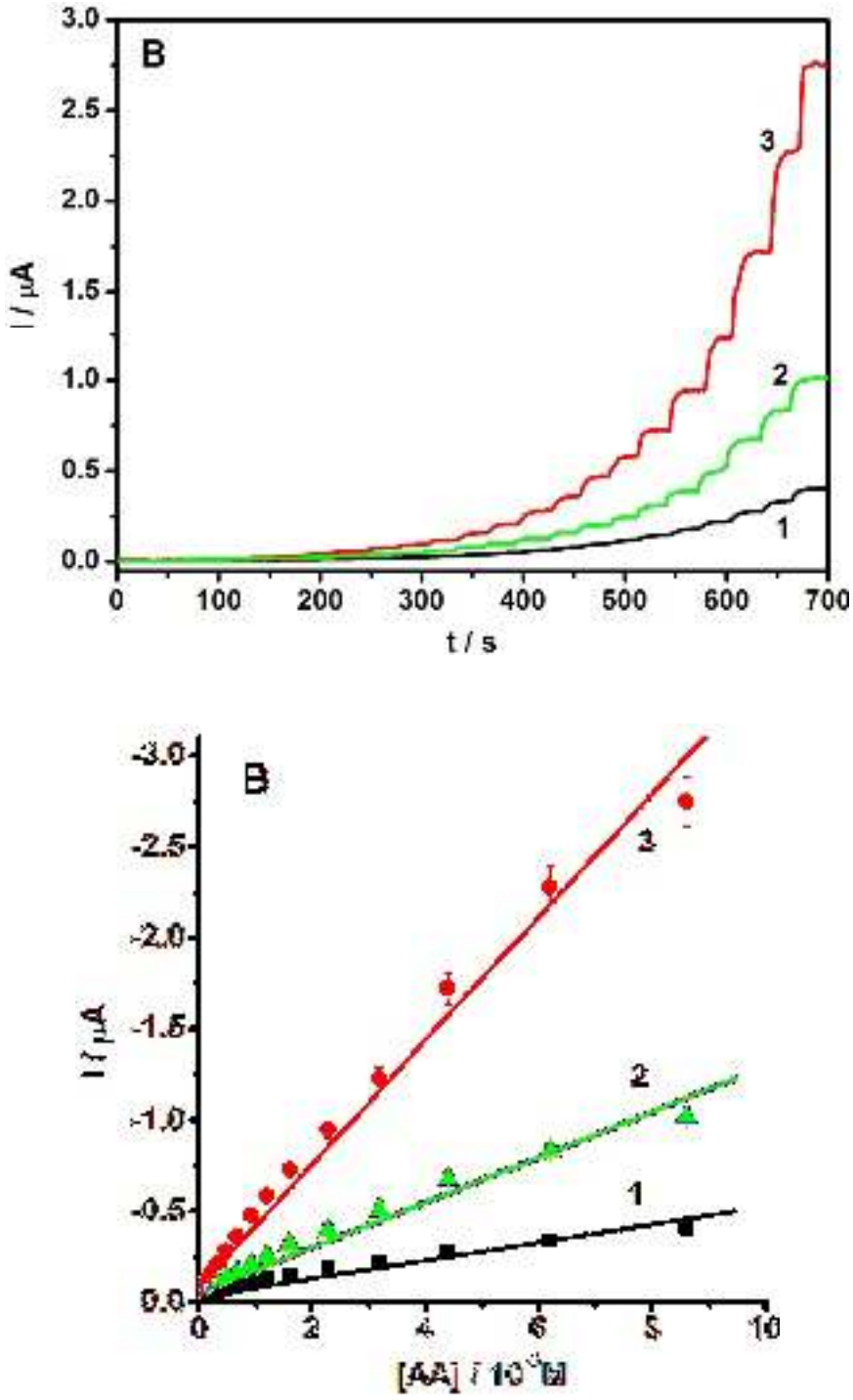

Figure 2.14. (A) Amperometric responses of the **(1)** Ormosil(FM), **(2)** Ormosil-TiO_2(FM) and **(3)** Ormosil-TiO_2-Pd(FM) systems on the addition of varying concentrations (10 nM to 5 mM) of AA in 0.1 M phosphate buffer(pH 7.0) at 0.3V vs. Ag/AgCl; **(B)** show the corresponding calibration curves for AA analysis.

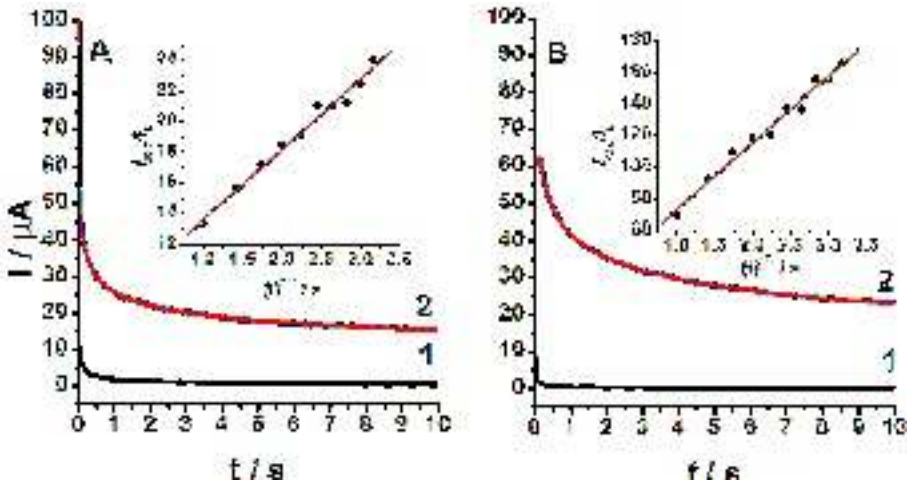

Figure 2.15. Chronoamperogram of Ormosil-TiO_2-Pd(Ferri) **(A)** and Ormosil-TiO_2-Pd(FM) **(B)** electrodes in absence **(1)** and the presence **(2)** of 1 mM of AA in 0.1 M phosphate buffer(pH 7.0). The insets to Figure 9A and Figure 9b show the plot of I_{cat}/I_L Vs. $t^{1/2}$.

2.3.7.2. *Amperometry*

Amperometric measurement was conducted for quantitative determination of AA, by successively adding AA (10 nM to 5 mM) at 0.3 V in 0.1 M phosphate buffer (pH 7.0) containing 0.5M KCl. Figure 2.13 A depicts the amperometric responses at varying concentrations of AA at (1) Ormosil(Ferri), (2) Ormosil-TiO_2(Ferri), (3) Ormosil-TiO_2-Pd(Ferri) systems. Similarly, Figure 2.14 A represent the amperometric responses at Ormosil(FM), Ormosil-TiO_2(FM), Ormosil-TiO_2-Pd(FM). The Figure 2.13 B and 2.14 B shows the corresponding calibration curves for AA analysis. The sensitivity of AA analysis was found to be 3.4, 7.27 and 19.92 $\mu AmM^{-1}cm^{-2}$ for Ormosil(Ferri), Ormosil-TiO_2(Ferri) and Ormosil-TiO_2-Pd(Ferri) system. Whereas, the sensitivity calculated for ferrocene methanol as mediator was found to be 6.05, 14.28 and 39.37$\mu AmM^{-1}cm^{-2}$ for Ormosil(FM), Ormosil-TiO_2(FM), Ormosil-TiO_2-Pd(FM). The Figure 2.13 B and 2.14 B shows the linear range of respective calibration curve. The results revealed the following information: (1) Gradual amplification in sensing response from Ormosil to Ormosil-TiO_2-Pd system; (2) better electro-catalytic behaviour of ferrocene methanol based system as compared to that of potassium ferricyanide.

2.3.7.3. *Chronoamperometry*

In support of above finding chronoamperometry was also used for the evaluation of the catalytic rate constant (kcat.). Figure 2.15 shows the chronoamperograms for the Ormosil-TiO_2-Pd(Ferri) [A] and Ormosil-TiO_2-Pd(FM) [B] electrodes in absence (1) and the presence (2) of 1 mM of AA by setting the step potential at 0.3 V vs. Ag/AgCl for subsequent evaluation of I_{cat} and I_L, where I_{cat} and I_L represent the currents of the modified electrode, in the presence and absence of AA respectively. The plot of I_{cat}/I_L vs. $t_{1/2}$ is shown in insets of Figure 2.15 A and 2.15 B for Ormosil-TiO_2-Pd(Ferri) and Ormosil-TiO_2-Pd(FM) electrode respectively. Over a limited time frame, the values of I_{cat}/I_L were linearly dependent on $t_{1/2}$, and from its slope k_{cat} was calculated. The values obtained were 4.23×10^2 and 6.24×10^3 M^{-1} s^{-1} for Ormosil-TiO_2-Pd(Ferri) (A) and Ormosil-TiO_2-Pd(FM) (B) system, respectively and again justify an enhance catalytic efficiency of Ormosil-TiO_2-Pd(FM) system toward AA oxidation.

2.3.8. *Stability and Reproducibility of Film*

The stability of the electrochemical performances of Ormosil-TiO_2-Pd(FM) electrode was studied . The Ormosil-TiO_2-Pd(FM) material have excellent stability showing less than 8% loss of electrochemical responses of electrode after 3 month. The stability of the mediator within the film is reasonable good for practical applications.

2.4. CONCLUSIONS

A comparative study on the synthesis of Ormosil, Ormosil-TiO_2, and Ormosil-TiO_2-Pd composite film is reported through various silane precursors under vigorous stirring and sonication. A smooth and non fragile homogeneous composite film with a continuous network structure is obtained with improved electrochemical and mechanical properties. The thickness of film controlled by concentration of TiO_2 and Pd linked glymo complex. The uniform and processible composite film formation of Ormosil-TiO_2-Pd with better chain interactions showed the potential of the material

towards various technological applications. The Ormosil-TiO_2-Pd composite film was found to be best in term of the electrochemical behavior in presence of two electron mediator potassium ferricyanide and ferrocene methanol. The Ormosil-TiO_2-Pd composite films were utilized for the development of electrochemical sensor thereby utilizing their functionality for practical application. The presence of TiO_2-Pd shows excellent electrocatalytic activity of ormosil for the oxidation of the biologically significant analyte like ascorbic acid (AA). The sensitivity was found to be six fold for ormosil-TiO_2-Pd(FM) and more than two fold for ormosil-TiO_2(FM) comparative than Ormosil electrode. The sensitivity of analysis to the order of $39.37\mu AmM^{-1}cm^{-2}$ with a linear detection range of 10nM to 1mM is recorded for ormosil-TiO_2-Pd(FM) electrode. The lowest detection limit for the oxidation of AA was found to be 50 nM for Ormosil-TiO_2-Pd(FM) electrode. The catalytic rate constant (k_{cat}) calculated by a linear graph between I_{cat}/I_L and $t_{1/2}$ obtained through chronoamperometry experiment. The value are found to the order of 6.24×10^3 M^{-1} s^{-1} for ormosil-TiO_2-Pd(FM) electrode. The electrochemical findings justify the role of TiO_2, TiO_2-Pd influencing the reversible redox behavior of mediators present within nanostructure domains of organically modified silicate.